ACS SENSORS

pubs.acs.org/acssensors

Article

Dynamic Solid-State Ultrasound Contrast Agent for Monitoring pH Fluctuations *In Vivo*

Julia Ann-Therese Walker, Xiaowei Wang, Karlheinz Peter, Kristian Kempe,* and Simon R. Corrie*

Cite This: *ACS Sens.* 2020, 5, 1190−1197

Read Online

ACCESS | Metrics & More | Article Recommendations | Supporting Information

ABSTRACT: The key challenge for *in vivo* biosensing is to design biomarker-responsive contrast agents that can be readily detected and monitored by broadly available biomedical imaging modalities. While a range of biosensors have been designed for optical, photoacoustic, and magnetic resonance imaging (MRI) modalities, technical challenges have hindered the development of ultrasound biosensors, even though ultrasound is widely available, portable, safe, and capable of both surface and deep tissue imaging. Typically, contrast-enhanced ultrasound imaging is generated by gas-filled microbubbles. However, they suffer from short imaging times because of the diffusion of the gas into the surrounding media. This demands an alternate approach to generate nanosensors that reveal pH-specific changes in ultrasound contrast in biological environments. Silica cores were coated with pH-responsive poly(methacrylic acid) (PMA_{SH}) in a layer-by-layer (LbL) approach and subsequently covered in a porous organosilica shell. Transmission electron microscopy (TEM) and confocal laser scanning microscopy (CLSM) were employed to monitor the successful fabrication of multilayered particles and prove the pH-dependent shrinkage/swelling of the PMA_{SH} layer. This demonstrates that reduction in pH below healthy physiological levels resulted in significant increases in ultrasound contrast, in gel phantoms, mouse cadaver tissue, and live mice. The future of such materials could be developed into a platform of biomarker-responsive ultrasound contrast agents for clinical applications.

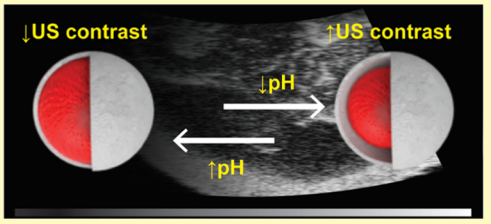

KEYWORDS: *ultrasound, nanosensor, biosensor, pH, mouse, layer-by-layer, silica, organosilica*

In vivo biosensing is an emerging research discipline in which the dynamic fluctuations of the critical biomarkers of health and disease are monitored in a continuous and real-time manner.[1] While the current paradigm of sample collection followed by endpoint analysis in a laboratory has served disease management well in many areas of medicine, the dynamic nature of some rapid onset conditions (*e.g.*, sepsis, acute coronary syndrome, ischemia/reperfusion injury, *etc.*) would significantly benefit from real-time monitoring. Several approaches to address this challenge have been demonstrated using different detection platforms, including the electrochemical sensing of therapeutic drug levels, the optical and electrochemical sensing of glucose in the management of diabetes, fluorescence imaging of cardiac ischemia/reperfusion injury using pH, and reactive oxygen species−sensitive nanoprobes, and the magnetic resonance imaging (MRI) of neurotransmitter-specific nanosensors.[2−11] However, optical systems suffer from poor depth penetration, electrochemical systems require "wiring" and provide no spatial information, and MRI (or positron-emission tomography) is not very feasible for real-time applications. There are enormous opportunities in developing new *in vivo* biosensors linked to simple and widely available detection techniques to provide timely information to guide therapeutic intervention.

Ultrasound is the most commonly used medical imaging technique as it is portable, noninvasive, and allows for tuneable tissue penetration.[12−14] Tissue discrimination in ultrasound can be enhanced by the use of contrast agents such as commercially available microbubbles (*ca.* 1−8 μm), which consist of a gaseous core and a phospholipid shell. Microbubbles for applications in molecular imaging is therefore a highly attractive field of research, for both diagnostic and theranostic applications.[15−19] However, these microbubbles have a short imaging time window (5−20 min after injection) due to gas diffusion, making them unsuitable for longer-term imaging or *in vivo* biosensing studies.[20,21] In more recent studies regarding contrast agent development, enzymes and inorganic agents have been incorporated into the interior of particles for the diagnostic detection of endogenous levels of hydrogen peroxide *in vivo*.[22−24] Although these ultrasound contrast agents do not suffer from the same fate as conventional ultrasound microbubbles, they are, however, still dose dependent and do not allow for continuous or "on-demand" monitoring.

Inorganic micro- and nanoparticles have attracted significant attention as echogenic contrast agents, due to their modular

Received: February 5, 2020
Accepted: March 23, 2020
Published: March 23, 2020

https://dx.doi.org/10.1021/acssensors.0c00245
ACS Sens. 2020, 5, 1190−1197

material properties (porosity, surface chemistry, *etc.*) and biocompatibility.[21,25−29] Silica can be fabricated into a wide array of sizes and shapes, with different porosities and core/shell structures, and also allows for the incorporation of organic, inorganic, and biological compounds. This versatility enables tuning of the scattering responses in ultrasound imaging through changing the density of the particles and number of interfaces.[26,28−31] With the exclusion of solid silica spheres, the silica materials applied in ultrasound imaging to date are dependent on the presence or generation of gas for ultrasound contrast.[28] This gas dependence for ultrasound signal transduction means that the materials are only suitable for diagnosis or monitoring in a short-term imaging window, opening up opportunities for stimuli-responsive, gas-independent materials for longer term, *e.g.*, monitoring of hydrogen peroxidase in the liver.[22,23]

The creation of hybrid materials between stimulus-responsive polymers and silica nanomaterials, in particular, has led to the development of contrast agents with enhanced mechanical strength, enhanced image contrast, and ultrasound-triggered drug release. The first generation of these materials featured microbubbles containing silane-polymer conjugates, designed either to strengthen the shell to reduce the rupture of particles,[31] or to incorporate enzyme substrates for triggered drug release.[29] More recently, mesoporous silica coated with thermoresponsive polymers has been used to control drug encapsulation and ultrasound-triggered release without premature drug leakage.[32] As an alternative to presynthesized polymer films, others have employed the layer-by-layer (LbL) process to create highly tuneable polymer capsules (altering number of layers, *etc.*) for drug encapsulation, which can be ruptured selectively in the ultrasound beam to release cargo.[13] LbL capsules infused with in situ−nucleated silica were also created to take advantage of the enhanced mechanical and contrast properties of the silica while maintaining the controlled release properties of the ultrasound-responsive polymer.[33] While the above-mentioned particles are capable of generating ultrasound contrast and can be utilized for theranostic or diagnostic applications, they are not suitable as ultrasound biosensors because they still exhibit gas diffusion and are susceptible to ultrasound beam damage.

While the combination of silica and polymeric nanomaterials has been used successfully to create new ultrasound contrast and controlled release agents, to the best of our knowledge, there are no reports of single-dose, nongas-dependent ultrasound *in vivo* biosensors, capable of producing a long-term reversible signal response to track dynamic changes in important biomarkers. In this study, we introduce a solid ultrasound nanosensor (sUN), capable of producing high imaging contrast in response to local pH differences in gel phantoms and animal tissue, without relying on gas production. While the healthy reference range for blood pH in adults is ∼7.3−7.45, pH varies with anatomical location (*e.g.*, 5.0−7.0 in the stomach) and disease states such as inflammatory disease, cancer, and transplant rejection.[34] In the case of tissue transplantation, the rejection for the transplant is associated with the pH decline to 6.45 or lower,[35] while acidified extracellular environments (pH < 7.0) are a hallmark of many cancers.[36]

The pH-responsive sUN designed in this study is composed of three critical building blocks: (i) a solid silica core, coated with (ii) a cross-linked thiol factionalized poly(methacrylic acid) (PMA_{SH}) multilayered film prepared by the hydrogen-bonded LbL technique, encapsulated by (iii) a porous organosilica shell. The separation of the two silica components by the dynamic PMA_{SH} film enables a reversible switch of scattering interfaces and a change in material properties in response to pH modulation, allowing for the real-time monitoring of pH by ultrasound imaging as demonstrated both *in vitro* and *in vivo*.

EXPERIMENTAL SECTION

Silica particles (SiO_2, 0.829 μm, 5 wt %) were purchased from microParticles GmbH. (3-Mercaptopropyl)trimethoxysilane (MPS, M_r 196.34 g mol^{-1}), triethylamine (TEA, M_r 101.19 g mol^{-1}), tannic acid (TA, M_r 1701.20 g mol^{-1}), poly(methacrylic acid) (PMAA, M_r 10 kDa, 30 wt %), poly(*N*-vinylpyrrolidone) (PVPON, M_r 40 kDa), sodium hydroxide (NaOH), dithiothreitol (DTT), 4-(4,6-dimethoxy-1,3,5-triazin-2-yl)-4-methylmorpholinium chloride (DMTMM), *N*-chloro-*p*-toluenesulfonamide sodium salt hydrate (chloramine-T hydrate), 2,2′-dithiodipyridine (DTDP), phosphate-buffered saline (PBS) tablets, 2-morpholinoethanesulfonic acid buffer (MES), sodium acetate (NaOAc), 3-(*N*-morpholino)propanesulfonic acid (MOPS), 4-(2-hydroxyethyl)-1-piperazineethanesulfonic acid (HEPES), agarose, and tetrahydrofuran were obtained from Sigma Aldrich. Cy5-maleimide (Cy5) was purchased from Lumiprobe. SYLGARD 184 silicone elastomer curing agent (poly(dimethylsiloxane) (PDMS)) was purchased from Dow Chemical. Alamar Blue and Dulbecco's modified Eagle's medium were purchased from ThermoFisher Scientific.

LbL and PMA_{SH} Postmodifications and sUN Synthesis. The LbL assembly of the thiol-linked poly(methacrylic acid) polymer (PMA_{SH}) was performed using a previously described method (Scheme S1).[22] Briefly, PMA_{SH} (3 mg) was dissolved in the DTT (20 μL, 0.5 mol) solution in the MOPS buffer (20 mM, pH 8) and stirred for 30 min at room temperature. The solution was then added to sodium acetate (40 mM, pH 4) buffer at a concentration of 100 g L^{-1} and adjusted to pH 4. PVPON was also dissolved at the concentration of 100 g L^{-1} in sodium acetate (40 mM, pH 4), and pH was adjusted to pH 4. The SiO_2 particles (100 μL, 5 wt %) were washed three times into sodium acetate (40 mM, pH 4) buffer and then incubated in the PVPON (200 μL, 1 mg mL^{-1}) solution for 10 min at room temperature. After the particles were washed three times, they were incubated with PMA_{SH} (200 μL, 1 mg mL^{-1}) for 10 min. This process was repeated until six bilayers were applied to the surface of the SiO_2 particles. The PMA_{SH} layers were cross-linked by the addition of chloramine T (1.26 mmol) in MES (50 mM, pH 6). The particles were then washed three times in the MES buffer to remove the PVPON layers and further washed three times into sodium acetate (40 mM, pH 4). To fluorescently label the polymer, Cy5 was dissolved in tetrahydrofuran (1.6 mM), 0.5 μL added to the particles suspended in NaOAc (500 μL, 40 mM, pH 4), incubated overnight, and subsequently washed three times to remove any unreacted dye. For shell coating, to hydrolyze the methoxy groups on MPS, milli-Q (80 mL) was acidized with hydrochloric acid (1.8 mL, 2 M) and MPS (10 mL) and was added and stirred (440 rpm) for 18 h. Following hydrolysis, this solution was split into two 50 mL falcon tubes and centrifuged (3500 RCF) for 30 min to separate aqueous monomers from higher-order oligomers. After washing SiO_2@$(PMA_{SH})_6$ (1.45×10^8 particles mL^{-1}) thoroughly first in PBS and then in 2× Milli-Q water, the shell coating reaction was initiated by adding hydrolyzed MPS (45 μL, 1.62 mM), TEA (1 μL, 3.19 mM), and TA (8.18×10^{-4} mM) in a final volume of 1.24 mL. This solution was then left to stir for 30 min, followed by extensive washing in Milli-Q water to remove unreacted reagents. Particle concentration was monitored throughout the study using a hemocytometer, based on three independent samples.

Confocal Laser Scanning Microscope. Confocal imaging was performed on a Leica SP8 X confocal using a 40× PL APO NA1.3 objective. All images were collected at zoom 3 and 2048 × 2048 pixel resolution to achieve optimal sampling. Excitation was performed by 633 nm laser lines with emission captured at 640−700 nm.

https://dx.doi.org/10.1021/acssensors.0c00245
ACS Sens. 2020, 5, 1190−1197

Scheme 1. Synthesis of pH-Responsive sUN[a]

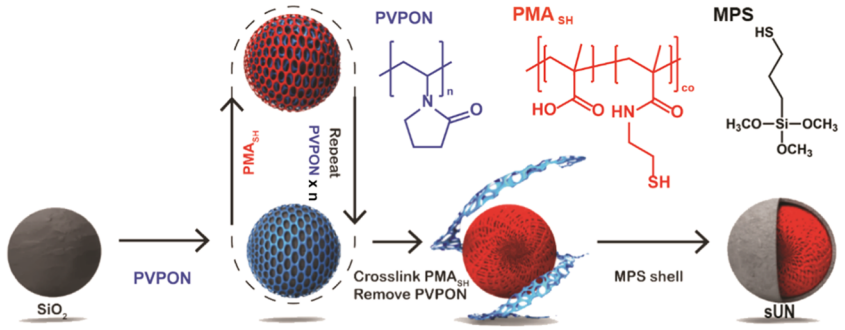

[a]Starting with the silica cores (SiO_2), PMA_{SH} and PVPON layers (six bilayers) were deposited in the LbL process. PMA_{SH} layers were cross-linked through the thiol functionality, and the PVPON was removed ($SiO_2@(PMA_{SH})_6$) subsequently. These particles were then encapsulated in a porous MPS shell to form the final sUN.

Fluorescence Microscopy. Fluorescence microscopy was performed on an Olympus BX 51 microscope equipped with a 100× objective lens (Olympus UPlanFL N 40 x/1.3, oil, Ph1). A charge-coupled device (CCD) camera (Olympus XM10) was mounted on the top port of the microscope. Fluorescence images (excitation: 604−644 nm, emission: 627−712 nm) were illuminated with a Hg arc lamp (Olympus U-RFL-T). Images were acquired using Cell Sens (Ver.1.18) and analyzed using ImageJ (version 2.35).

Electron Microscopy. The transmission electron microscopy (TEM) images of the particles were collected using the FEI Tecnai T20 with a LaB6 emitter and twin lens using an acceleration voltage of 200 kV. The images were acquired using an Orius SCD200D wide-angle CCD camera. Samples were prepared by drying aqueous particle suspension onto holy carbon grids mounted onto a single tilting holder. To prepare microtomed sections, sUNs were freeze-dried for 24 h, then embedded into a resin, sliced into ∼90-nm-thick sections (Ultracut S microtome, Reichert-Leica) and mounted on a holey carbon copper grid (200 mesh, ProSciTech).

Gel Phantom Preparation for Ultrasound Imaging. The mold used for phantom measurements was designed in Rhinoceros 5 and converted to .stl file format following three-dimensional (3D) printing on a FLASHFORGE NEW Creator Pro Dual Extrusion 3D Printer in acrylonitrile butadiene styrene (see Figure S4a). PDMS set with 10% of cross-linking agent was poured into a 3D-printed mold in a desiccator and kept under vacuum for 24 h, to ensure that cross-linking had occurred, before being placed in an oven for 60 min (see resulting mold, Figure S4b). To prepare agarose phantoms, the HEPES buffer (40 mM, pH 7) was degassed three times to remove any air bubbles. The HEPES buffer (50 mL, 40 mM, pH 7) was then heated to 90 °C under constant stirring, and then agarose (100 mg) was added to the solution. After the agarose was dissolved, the temperature was lowered to 80 °C for 30 min. The sUN particles were then resuspended into the degassed HEPES buffer (40 mM, pH 7). Without introducing gas bubbles, a particle suspension (10 μL, 4 × 10^5 particles mL^{-1}) was mixed with an equal volume of buffered agarose. Then the suspension was pipetted into a cylindrical tube mold and left to set for 10 min before being removed and resuspended in the HEPES buffer (40 mM, pH 7). Each sample was prepared in triplicate. For ultrasound imaging, the phantoms were placed onto a surface coated with ultrasound gel. Images from gel phantoms were acquired using the FIJIFILM VisualSonics Vevo 2100 instrument, with the MS-550D transducer at 40 MHz. Subsequently, gel phantoms were washed thoroughly in the HEPES buffer (40 mM) at the desired pH to remove the residual gel and stored at 4 °C for reimaging over several days. The controls of SiO_2 cores in agar were prepared and imaged using the same method.

***In Vitro* Cell Viability Assay.** Cell viability was assessed via the Alamar Blue assay. Cells were seeded the day before on 96-well plates at a density of 10 000 cells per well. The cells were then incubated with sUN samples (1.12 × 10^8 particles mL^{-1}) in PBS, prepared through serial dilution and incubated at 37 °C for 24 h in a humidified incubator with 5% of atmospheric CO_2. The samples were run in triplicate. After incubation, the medium was removed and a 10% v/v solution of Alamar Blue in Dulbecco's modified Eagle's medium was added. The cells were incubated for a further 4 h at 37 °C. Cell viability was determined by measuring the fluorescence (excitation: 540 nm, emission: 590 nm). Wells incubated without cells were used as blank. Control samples were cells incubated with PBS (without sUN).

Ultrasound Imaging and Data Analysis. Ultrasound images were acquired by the FUJIFILM VisualSonics Vevo 2100 instrument, using the MS-550D transducer at 40 MHz (gel phantoms and cadavers) and the MX250 transducer at 18 MHz 10% dB power and 2D gain at 15 (live animals). Images were analyzed using ImageJ, whereby each sample was recorded in a .avi stack frame that contained no artifacts (air bubbles or mold reflections). On each image stack, manual regions of interest (ROI) were drawn on the inital image and applied though sucsessive stacks for pH 4, 5, 6, and 7 and the background and control, avoiding interfaces. The average integrated densities were collected, and the background signal (before injections) was subtracted. For cadaver images, from a series of 10 frames to avoid artifacts from the needle, ROI were drawn in ImageJ and the average of the integrated density was calculated.

Animal Studies. Cadaver experiments were carried out on freshly culled 8 week female athymic Balb/C nude mice, following exsanguination using heparinized saline (10 μL mL^{-1}, 8 mL of total infusion volume) to remove the blood volume. Twin subcutaneous perfusion lines were applied to the flank for particle and buffer injections. The degassed HEPES buffer (200 μL, 40 mM, pH 4) was injected into the cadaver from one line, and subsequently, sUN or silica cores (25 μL, 1.12 × 10^8 particles mL^{-1}) were injected in the second line which was then removed from the skin. The site was monitored for 1 h with a 3D scan acquired every 10 min, followed by the injections of the degassed HEPES buffer (200 μL, 40 mM, pH 4), with the last injection of the HEPES buffer (200 μL, 40 mM, pH 7). Live animal imaging experiments were performed on C57/black mice in accordance with the Australian Code for the care and use of animals for scientific purposes and approved by the AMREP Animal Ethics Committee. Following isoflurane, hair removal cream was applied to the flank of the mouse before imaging; subsequently, sUN or silica cores (50 μL, 1.12 × 10^8 particles mL^{-1}) suspended in the PBS (0.1 M, pH 7) buffer were mixed with acidized PBS (50 μL, 0.1 M, pH 3.2) and then immediately injected into the flank skin via subcutaneous injection. Brightness mode and contrast mode ultrasound imaging were performed immediately after injection, and every 5 min for 15 min.

RESULTS AND DISCUSSION

Synthesis and Characterization of sUNs. To create an sUN responsive to local pH changes, we designed a multilayered nanoparticle, encasing a pH-sensitive polymer

https://dx.doi.org/10.1021/acssensors.0c00245
ACS Sens. 2020, 5, 1190−1197

film in between a silica core and a porous organosilica shell (Scheme 1). To this end, poly(vinylpyrrolidone) (PVPON) and thiol-modified PMA (PMA_{SH}) were alternatively deposited onto the surface of the silica cores via a hydrogen-bonding LbL approach (Scheme S1).[37,38] Upon successful layer build-up, PMA_{SH} layers were cross-linked through the oxidation of the free thiols, and PVPON was removed by washing into PBS (pH 7.4). The degree of thiol functionality in PMA_{SH} layers has been reported to affect the degree of swelling in the resulting polymer films.[39−41] Here we chose a polymer with 10 mol % thiol functionality, to allow the pH-responsive swelling of films to occur.[40] Finally, to provide an additional interface and also to protect the critical polymer film, we encapsulated $SiO_2@(PMA_{SH})_6$ in an organosilica shell primarily composed of 3-mercaptopropyltrimethoxysilane (MPS). The shell was deposited using tannic acid as a porogen, under conditions favoring polymer film expansion (pH 7.4), thus allowing for proton transport through the shell to the responsive polymer. A combination of confocal fluorescence and transmission electron microscopy was employed to characterize the nanomaterials at different stages of fabrication. To study the PMA_{SH}-modified SiO_2 core particles after cross-linking, the polymer film was labeled with Cy5 maleimide on the residual free thiols on the PMA_{SH} polymer by the maleimide−thiol coupling reaction. The polymer film thickness was observed to vary as a function of pH, based on confocal microscopy observations (Figure 1a,b).

As the pK_a of the PMA_{SH} film is ~4.9,[40] the acid groups are deprotonated under neutral or physiological pH, causing the swelling of the film due to repulsion between the negatively charged carboxylate groups, whereas in acidic conditions below the pK_a, the acid groups are protonated, and the film is contracted onto the silica cores. In solution, the size of the overall particle varied between 1.91 ± 0.02 μm at pH 7 and 1.67 ± 0.03 μm at pH 4, consistent with previous reports.[39] The MPS shell was coated onto the expanded polymer-coated silica cores at pH 7, to retain the interstitial space between the shell and core, allowing for the expansion and contraction of PMA_{SH} during sensor application. Interestingly, once the porous MPS shell was synthesized on the top of the polymer-coated cores, we observed a negligible change in particle size as a function of pH, indicating that the shell has a constraining effect on the swelling behavior of the polymer film (Figure S1). TEM revealed that the polymer film after cross-linking is visible as a thin film coating the core (Figure 1d,e). The MPS shell coating was also confirmed by TEM, indicating a rougher surface (Figure 1d,e) along with a change in size from silica cores of a mean diameter of 840 ± 0.71 to 1.1 ± 0.12 μm (Figure 1f). Moreover, microtome TEM images confirmed the presence of three distinct material layers on the surface of the SiO_2 cores, with the PMA_{SH} film covering the entirety of the silica core and a thin silica shell layer present on the edges of the polymer (Figure S3). Note that the change in size observed in TEM is not consistent with that in confocal microscopy due to material shrinkage under high vacuum.

Echogenic Properties of sUNs in Gel Phantoms. Upon the successful fabrication of the sUN, agarose gel phantoms were prepared and imaged with a preclinical ultrasound imaging system to evaluate changes in contrast intensity under different pH conditions. A custom-designed, ultrasound-neutral poly(dimethylsiloxane) (PDMS) device was cast as the sample holder (Figure S4a,b), allowing for the 3D alignment of the sample to maintain a constant distance

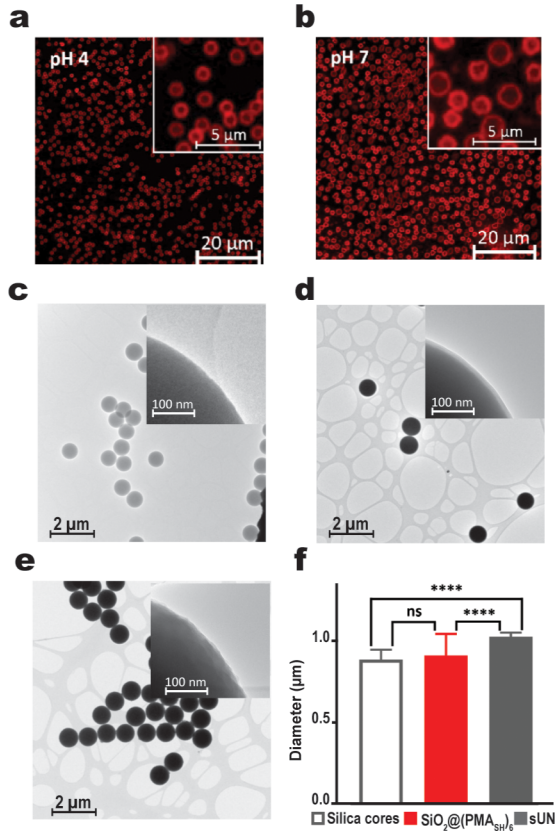

Figure 1. Microscopic characterization of silica cores and sUN. Confocal microscopy of Cy5-labeled $SiO_2@(PMA_{SH})_6$ in 40 mM HEPES buffer at (a) pH 4 and (b) pH 7. TEM images of (c) SiO_2 cores, (d) $SiO_2@(PMA_{SH})_6$ showing a polymer film deposited on the surface of the SiO_2 cores, and (e) sUN following the addition of the silica layer on the top of the PMA_{SH} film. (f) Size distribution of SiO_2, $SiO_2@(PMA_{SH})_6$, and sUN, measured on TEM micrographs (****P < 0.0001).

from the transducer. Gel phantoms were prepared to contain either sUN or SiO_2 negative control samples. First, the phantoms containing sUNs at pH 7 were imaged every 24 h over 3 days, confirming a long-term, stable echogenic response (Figure 2a), in comparison to a shorter-lived gas-filled polymer or silica-based microbubbles.[21,25,30,42,43] Next, the sUNs and

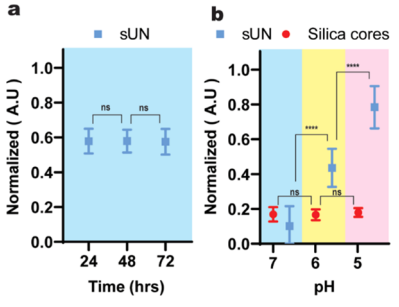

Figure 2. Ultrasound imaging of nanoparticle-encapsulated gel phantoms. (a) Effect of time on the ultrasound signal of sUN suspended in agar (1%) in the HEPES buffer (40 mM) at pH 7, imaged over 72 h at 24 h time points. (b) Effect of pH on ultrasound response for SiO_2 cores (control) compared to sUN, suspended in agar (1%) in the HEPES buffer (40 mM), showing the relationship between pH and ultrasound backscatter (****P < 0.0001).

https://dx.doi.org/10.1021/acssensors.0c00245
ACS Sens. 2020, 5, 1190−1197

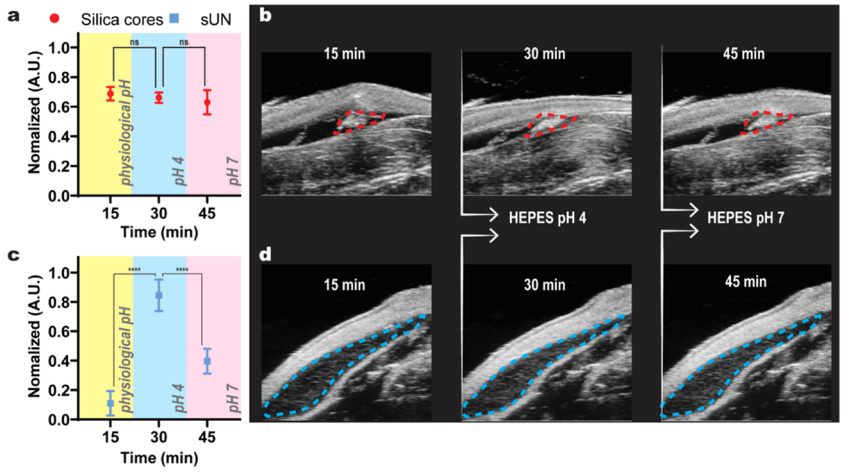

Figure 3. Ultrasound imaging of control and sUN in tissue. (a) Corresponding gray values of the control, taken from the region of interest (ROI) measured at 15 min time points as integrated density over the image stacks, showing no statistical difference in ultrasound backscatter with the change of pH. (b) *Ex vivo* ultrasound images of SiO_2 cores (control) following the same protocol as sUNs (b). (c) Corresponding gray values of the sUN, taken from the region of interest (ROI) measured at 15 min time points as integrated density over the image stacks ****$P < 0.0001$, ns $P < 0.9421$. (d) *Ex vivo* ultrasound images of sUN injection into the subcutaneous tissue with HEPES buffer at pH 4; after 15 min, a further 100 μL of HEPES (pH 4) was injected; at 30 min, 100 μL of HEPES (pH 7) was injected.

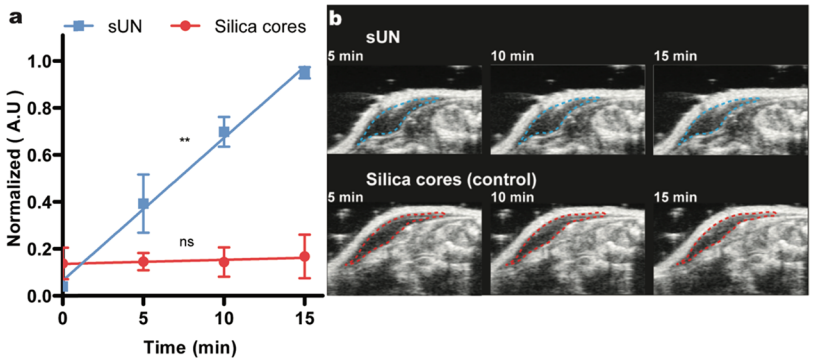

Figure 4. Ultrasound imaging of sUN *in vivo*. (a) Plots of the corresponding normalized gray values of sUNs and silica cores, taken from an area of injection, measured at 5 min time points as integrated density over the image stacks. Statistical analysis indicated a nonzero slope for sUNs ($P = 0.0028$), in comparison to the silica cores ($P = 0.1458$). (b) Corresponding representative ultrasound images for points plotted in (a).

SiO_2 control phantoms were imaged after incubation in buffer at pH 7, 6, and 5. We observed a 2-fold increase in ultrasound contrast with each decreasing step in pH for the sUNs, while the corresponding signal of the SiO_2 control samples did not change significantly with pH (Figure 2b). To our knowledge, this is the first example of analyte-dependent contrast enhancement without reliance on a gas-based system. The pH dependence of the ultrasound signal for the sUNs is likely based on two complementary mechanisms.

First, the stiffness of PMA_{SH} layers formed through the LbL process on surfaces has been shown to increase dramatically with decreasing pH.[44] However, the gap required for the expansion and contraction of PMA_{SH} between the silica core and organosilica shell remains relatively constant (based on observed size trends, Figure S1). Previously, it was shown that hard inclusions in a soft medium would have a high level of contrast-transfer efficiency, and the transfer efficiency decreases with decreasing density.[12,45] Hence the pH-dependent stiffness of the polymer layer would translate to a density change, leading to ultrasound enhancement at low pH (based on harmonic trends, Figure S2). Second, increasing the number of interfaces for scattering or reflection in a multicompartment silica nanomaterial has also been observed to increase an ultrasound signal.[28] This could also partly explain the increased ultrasound signal at low pH for the sUNs; when the PMA_{SH} layer is contracted against the core, there are two clear silica interfaces at which scattering/reflection could occur, whereas when the PMA_{SH} is expanded, it could act to reduce this effect.[28]

Ultrasound Imaging of sUNs in Animal Tissue. We next investigate pH-responsive ultrasound contrast imaging in mouse cadavers. Images were collected from subcutaneous tissue in the flank skin of mice, in an area which showed minimal ultrasound contrast upon injection. Imaging was carried out before and after the subcutaneous injection of sUN or SiO_2 controls, and following simulated pH changes via the injection of HEPES buffer solutions at pH 4 or 7. For the evaluation of the images, we used a manually defined region of interest (ROI).[23,46] This region was defined from the last data set in the series, which was then extrapolated to the remaining data sets in that series. The background for subtraction was based on the same tissue site before nanoparticle injection. The SiO_2 controls showed a negligible change in ultrasound contrast during the experiment (45 min, Figure 3a,b), in agreement with phantom experiments. The sUNs initially injected at physiological pH showed low signal, which

https://dx.doi.org/10.1021/acssensors.0c00245
ACS Sens. 2020, 5, 1190−1197

increased upon injection at pH 4. Reversing the pH value to 7 caused a significant drop in signal (Figure 3c,d). These results show that sUNs could produce reversible pH-specific changes in ultrasound contrast in animal tissue, over at least 45 min of imaging time.

Progressing from cadaver studies, we next investigated the pH-responsiveness of sUNs in live animals in comparison to SiO_2 core controls. At this point, before live animal imaging, we also evaluated the cytotoxicity of the sUNs on NIH/3T3 cells using an Alamar Blue assay. The sUN particles showed negligible toxicity on the cells in comparison to the control (Figure S5), consistent with recent studies from our groups and others on the biocompatibility of organosilica materials.[47−49] sUNs and cores were initially injected into the flank skin of mice in the PBS pH 7 buffer, followed by an injection of low-pH PBS to transiently reduce the local tissue pH. Images were collected every 5 min over 15 min, and we observed a significant increase in contrast for the sUNs in comparison to a constant signal for the silica cores (Figure 4). This suggests that the average pH in the injection area decreased over the 15 min imaging period. To further investigate the sUN stability in the ultrasound beam in live animals, a triggered pulse sequence was employed, which typically resulted in the bursting of microbubbles.[13] Yet, no change in image contrast or harmonic signals was observed, suggesting that the sUNs were mechanically stable during typical pulse sequences (Figure S6).

With the combination of deep tissue penetration and widespread utility, ultrasound imaging could be a "gateway" modality for the clinical translation of *in vivo* biosensing technologies. The diagnostic applications of ultrasound traditionally involve imaging of blood flow and/or movement of anatomical structures; however, in this study, we created a long sought-after link to functional molecular imaging, which when combined with long-term material stability and reversibility leads to a unique *in vivo* biosensing approach. In comparison to fluorescence modalities, which are currently the leading technologies in this area,[3,7,8] our results point to several additional advantages beyond those previously introduced. First, there is no need to incorporate fluorophores, several of which are potentially cytotoxic and have recently been shown to affect cellular trafficking *in vivo*.[50−52] The image analysis from ultrasound imaging is also more straightforward than for fluorescence, as there is no need for spectral unmixing algorithms. Finally, we found that we could tailor the material properties of the nanosensors directly for the preclinical/clinical imaging system, rather than for a lab-based imaging system that may have different requirements for clinical applications (*e.g.*, a fluorescence microscope vs a fluorescent imaging camera).[6,9] However, it is not yet possible to undertake multiplexing analysis with ultrasound, a common practice in fluorescent measurements, but the field is ripe for future development that may include photoacoustic detection approaches or materials with unique radio frequency signals to begin addressing this limitation in the future. The next step in this research is to progress our animal studies from technical proof-of-concept to investigating dynamic pH changes in animal models of disease, including investigation on biodistribution from the implantation site, and the potential inflammatory reactions of host tissue toward the sUN sensor, with the key goal to translate the technology into human imaging studies.

CONCLUSIONS

In this study, we have demonstrated the fabrication of a solid, gas-free ultrasound contrast agent that produced a pH-dependent contrast enhancement response *in vivo*. After fabricating and characterizing a hybrid silica/PMA_{SH} nanomaterial, we then showed clear pH-dependent contrast enhancement in gel phantoms along with signal stability over at least three days, in comparison to microbubbles, which show relatively short imaging times due to either diffusion of gas into the bloodstream or bursting of the bubble during imaging.[24] We then injected and imaged the particles in mouse tissue samples and live mice, observing clear pH-dependent signals over relatively long imaging times, without bursting behavior, in comparison to PMA_{SH}-free silica controls. These materials hold strong promise for biomarker-responsive ultrasound imaging agents to be ultimately used in patients.

ASSOCIATED CONTENT

Supporting Information

The Supporting Information is available free of charge at https://pubs.acs.org/doi/10.1021/acssensors.0c00245.

Synthesis scheme, fluorescence microscopy analysis, TEM images, design and images of phantom holder, cell toxicity data and pulsed ultrasound harmonic images and graph (PDF).

AUTHOR INFORMATION

Corresponding Authors

Kristian Kempe − *ARC Centre of Excellence in Convergent Bio-Nano Science and Technology, and Drug Delivery, Disposition and Dynamics, Monash Institute of Pharmaceutical Sciences and Materials Science and Engineering, Monash University, Parkville, VIC 3052, Australia;* orcid.org/0000-0002-0136-9403; Email: Kristian.kempe@monash.edu

Simon R. Corrie − *ARC Centre of Excellence in Convergent Bio-Nano Science and Technology, Chemical Engineering, Monash University, Clayton, VIC 3800, Australia;* orcid.org/0000-0001-8029-1896; Email: Simon.corrie@monash.edu

Authors

Julia Ann-Therese Walker − *ARC Centre of Excellence in Convergent Bio-Nano Science and Technology, Chemical Engineering and ARC Centre of Excellence in Convergent Bio-Nano Science and Technology, and Drug Delivery, Disposition and Dynamics, Monash Institute of Pharmaceutical Sciences, Monash University, Clayton, VIC 3800, Australia*

Xiaowei Wang − *Baker Heart and Diabetes Institute, Melbourne, VIC 3004, Australia; Department of Medicine, Monash University, Melbourne 3800, Australia*

Karlheinz Peter − *Baker Heart and Diabetes Institute, Melbourne, VIC 3004, Australia; Department of Medicine, Monash University, Melbourne 3800, Australia*

Complete contact information is available at: https://pubs.acs.org/10.1021/acssensors.0c00245

Author Contributions

J.W. designed the research plan and performed all experiments. J.W., K.K., and S.C. designed the sensor. X.W. carried out the *in vivo* experiments including animal surgery with J.W. assisting with the data recording. J.W. processed all experimental data. J.W., K.K., and S.C. wrote the manuscript with contributions

https://dx.doi.org/10.1021/acssensors.0c00245
ACS Sens. 2020, 5, 1190−1197

from X.W. and K.P. All authors read and approved the final manuscript.

Notes

The authors declare no competing financial interest.

■ ACKNOWLEDGMENTS

The authors acknowledge the use of the facilities and the assistance of Dr. T. Williams, Dr. Y. Chen, and Dr. R. King at the Monash Center for Electron Microscopy. They would also like to acknowledge Dr. M. De Veer and Dr. E. Salimova at Monash Biomedical Imaging for their assistance and use of facilities. The authors further acknowledge and thank Dr. O. Feeney, A. M. Mahmoud, and D. Brundel and Dr. C.J. Nowell from Monash Institute of Pharmaceutical Sciences and Dr. K. J. Robinson from Chemical Engineering at Monash University for their contributions to this project.

■ REFERENCES

(1) Rong, G.; Corrie, S. R.; Clark, H. A. In Vivo Biosensing: Progress and Perspectives. *ACS Sens.* **2017**, *2*, 327−338.
(2) Lubin, A. A.; Plaxco, K. W. Folding-Based Electrochemical Biosensors: The Case for Responsive Nucleic Acid Architectures. *Acc. Chem.* **2010**, *43*, 496−505.
(3) Bornhoeft, L. R.; Biswas, A.; McShane, M. J. Composite Hydrogels with Engineered Microdomains for Optical Glucose Sensing at Low Oxygen Conditions. *Biosenors* **2017**, *7*, No. 8.
(4) Nayak, S. R.; McShane, M. J. Fluorescence glucose monitoring based on transduction of enzymatically-driven pH changes within microcapsules. *Sens. Lett.* **2006**, *4*, 433−439.
(5) Zhu, H. G.; Srivastava, R.; Brown, J. Q.; McShane, M. J. Combined physical and chemical immobilization of glucose oxidase in alginate microspheres improves stability of encapsulation and activity. *Bioconjugate Chem.* **2005**, *16*, 1451−1458.
(6) Scholten, K.; Meng, E. A review of implantable biosensors for closed-loop glucose control and other drug delivery applications. *Int. J. Pharm.* **2018**, *544*, 319−334.
(7) Kim, E. H.; Chin, G.; Rong, G. X.; Poskanzer, K. E.; Clark, H. A. Optical Probes for Neurobiological Sensing and Imaging. *Acc. Chem. Res.* **2018**, *51*, 1023−1032.
(8) Williams, R. M.; Lee, C.; Galassi, T. V.; Harvey, J. D.; Leicher, R.; Sirenko, M.; Dorso, M. A.; Shah, J.; Olvera, N.; Dao, F.; Levine, D. A.; Heller, D. A. Noninvasive ovarian cancer biomarker detection via an optical nanosensor implant. *Sci. Adv.* **2018**, *4*, No. eaaq1090.
(9) Arroyo-Currás, N.; Somerson, J.; Vieira, P. A.; Ploense, K. L.; Kippin, T. E.; Plaxco, K. W. Real-time measurement of small molecules directly in awake, ambulatory animals. *Proc. Natl. Acad. Sci. U.S.A.* **2017**, *114*, 645−650.
(10) Luo, Y.; Kim, E. H.; Flask, C. A.; Clark, H. A. Nanosensors for the Chemical Imaging of Acetylcholine Using Magnetic Resonance Imaging. *ACS Nano* **2018**, *12*, 5761−5773.
(11) Ziegler, M.; Xu, X.; Yap, M. L.; Hu, H.; Zhang, J.; Peter, K. A Self-Assembled Fluorescent Nanoprobe for Imaging and Therapy of Cardiac Ischemia/Reperfusion Injury. *Adv. Ther.* **2019**, *2*, No. 1800133.
(12) Sigrist, R. M. S.; Liau, J.; El Kaffas, A.; Chammas, M. C.; Willmann, J. K. Ultrasound Elastography: Review of Techniques and Clinical Applications. *Theranostics* **2017**, *7*, 1303−1329.
(13) Chen, J.; Ratnayaka, S.; Alford, A.; Kozlovskaya, V.; Liu, F.; Xue, B.; Hoyt, K.; Kharlampieva, E. Theranostic Multilayer Capsules for Ultrasound Imaging and Guided Drug Delivery. *ACS Nano* **2017**, *11*, 3135−3146.
(14) Jokerst, J. V.; Gambhir, S. S. Molecular Imaging with Theranostic Nanoparticles. *Acc. Chem. Res.* **2011**, *44*, 1050−1060.
(15) Wang, X. W.; Gkanatsas, Y.; Palasubramaniam, J.; Hohmann, J. D.; Chen, Y. C.; Lim, B.; Hagemeyer, C. E.; Peter, K. Thrombus-Targeted Theranostic Microbubbles: A New Technology towards Concurrent Rapid Ultrasound Diagnosis and Bleeding-free Fibrinolytic Treatment of Thrombosis. *Theranostics* **2016**, *6*, 726−738.
(16) Wang, S.; Hossack, J. A.; Klibanov, A. L. Targeting of microbubbles: contrast agents for ultrasound molecular imaging. *J. Drug Targeting* **2018**, *26*, 420−434.
(17) Wang, X.; Hagemeyer, C. E.; Hohmann, J. D.; Leitner, E.; Armstrong, P. C.; Jia, F.; Olschewski, M.; Needles, A.; Peter, K.; Ahrens, I. Novel single-chain antibody-targeted microbubbles for molecular ultrasound imaging of thrombosis: validation of a unique noninvasive method for rapid and sensitive detection of thrombi and monitoring of success or failure of thrombolysis in mice. *Circulation* **2012**, *125*, 3117−26.
(18) Wang, X.; Searle, A. K.; Hohmann, J. D.; Liu, A. L.; Abraham, M. K.; Palasubramaniam, J.; Lim, B.; Yao, Y.; Wallert, M.; Yu, E. F.; Chen, Y. C.; Peter, K. Dual-Targeted Theranostic Delivery of miRs Arrests Abdominal Aortic Aneurysm Development. *Mol. Ther.* **2018**, *26*, 1056−1065.
(19) Knowles, J. A.; Heath, C. H.; Saini, R.; Umphrey, H.; Warram, J.; Hoyt, K.; Rosenthal, E. L. Molecular Targeting of Ultrasonographic Contrast Agent for Detection of Head and Neck Squamous Cell Carcinoma. *Arch. Otolaryngol., Head Neck Surg.* **2012**, *138*, 662−668.
(20) Opacic, T.; Dencks, S.; Theek, B.; Piepenbrock, M.; Ackermann, D.; Rix, A.; Lammers, T.; Stickeler, E.; Delorme, S.; Schmitz, G.; Kiessling, F. Motion model ultrasound localization microscopy for preclinical and clinical multiparametric tumor characterization. *Nat. Commun.* **2018**, *9*, No. 1527.
(21) Huang, C. H.; Wang, J.; Yang, J.; Oviedo, J. P.; Na, M. S.; Trogler, W. C.; Blair, S. L.; Kim, M. J.; Kummel, A. C. Thickness and Sphericity Control of Hollow Hard Silica Shells through Iron (III) Doping: Low Threshold Ultrasound Contrast Agents. *Adv. Funct. Mater.* **2019**, *29*, No. 1900893.
(22) Guo, J. L.; Wang, X. W.; Henstridge, D. C.; Richardson, J. J.; Cui, J. W.; Sharma, A.; Febbraio, M. A.; Peter, K.; de Haan, J. B.; Hagemeyer, C. E.; Caruso, F. Nanoporous Metal-Phenolic Particles as Ultrasound Imaging Probes for Hydrogen Peroxide. *Adv. Healthcare Mater.* **2015**, *4*, 2170−2175.
(23) Olson, E. S.; Ortac, I.; Malone, C.; Esener, S.; Mattrey, R. Ultrasound Detection of Regional Oxidative Stress in Deep Tissues Using Novel Enzyme Loaded Nanoparticles. *Adv. Healthcare Mater.* **2017**, *6*, No. 1601163.
(24) Zhu, J. Z.; Li, Z. C.; Zhang, C. C.; Lin, L.; Cao, S. P.; Che, H. L.; Shi, X. Y.; Wang, H.; van Hest, J. C. M. Single enzyme loaded nanoparticles for combinational ultrasound-guided focused ultrasound ablation and hypoxia-relieved chemotherapy. *Theranostics* **2019**, *9*, 8048−8060.
(25) Liberman, A.; Wang, J.; Lu, N.; Viveros, R. D.; Allen, C. A.; Mattrey, R. F.; Blair, S. L.; Trogler, W. C.; Kim, M. J.; Kummel, A. C. Mechanically Tunable Hollow Silica Ultrathin Nanoshells for Ultrasound Contrast Agents. *Adv. Funct. Mater.* **2015**, *25*, 4049−4057.
(26) Blum, N. T.; Yildirim, A.; Gyorkos, C.; Shi, D.; Cai, A.; Chattaraj, R.; Goodwin, A. P. Temperature-Responsive Hydrophobic Silica Nanoparticle Ultrasound Contrast Agents Directed by Phospholipid Phase Behavior. *ACS Appl. Mater. Interfaces* **2019**, *11*, 15233−15240.
(27) Casciaro, S.; Conversano, F.; Ragusa, A.; Malvindi, M. A.; Franchini, R.; Greco, A.; Pellegrino, T.; Gigli, G. Optimal Enhancement Configuration of Silica Nanoparticles for Ultrasound Imaging and Automatic Detection at Conventional Diagnostic Frequencies. *Invest. Radiol.* **2010**, *45*, 715−724.
(28) Zhang, K.; Chen, H. R.; Guo, X. S.; Zhang, D.; Zheng, Y. Y.; Zheng, H. R.; Shi, J. L. Double-scattering/reflection in a Single Nanoparticle for Intensified Ultrasound Imaging. *Sci. Rep.* **2015**, *5*, No. 8766.
(29) Tsao, N. H.; Hall, E. A. H. Enzyme-Degradable Hybrid Polymer/Silica Microbubbles as Ultrasound Contrast Agents. *Langmuir* **2016**, *32*, 6534−6543.
(30) Liberman, A.; Wu, Z.; Barback, C. V.; Viveros, R. D.; Wang, J.; Ellies, L. G.; Mattrey, R. F.; Trogler, W. C.; Kummel, A. C.; Blair, S. L.

Hollow iron-silica nanoshells for enhanced high intensity focused ultrasound. *J. Surg. Res.* **2014**, *190*, 391−398.
(31) Lin, P. L.; Eckersley, R. J.; Hall, E. A. H. Ultrabubble: A Laminated Ultrasound Contrast Agent with Narrow Size Range. *Adv. Mater.* **2009**, *21*, 3949.
(32) Paris, J. L.; Cabanas, M. V.; Manzano, M.; Vallet-Regi, M. Polymer-Grafted Mesoporous Silica Nanoparticles as Ultrasound-Responsive Drug Carriers. *ACS Nano* **2015**, *9*, 11023−11033.
(33) Gao, H.; Wen, D.; Sukhorukov, G. B. Composite silica nanoparticle/polyelectrolyte microcapsules with reduced permeability and enhanced ultrasound sensitivity. *J. Mater. Chem. B* **2015**, *3*, 1888−1897.
(34) Lopez, J. *Tietz Fundamentals of Clinical Chemistry and Molecular Diagnostics*, 7th ed.; Elsevier, 2014.
(35) Dunn, R. M.; Kaplan, I. B.; Mancoll, J.; Terzis, J. K.; Trengovejones, G. Experimental and clinican use of pH monitoring of free tissue transfers. *Ann. Plast. Surg.* **1993**, *31*, 539−545.
(36) Kato, Y.; Ozawa, S.; Miyamoto, C.; Maehata, Y.; Suzuki, A.; Maeda, T.; Baba, Y. Acidic extracellular microenvironment and cancer. *Cancer Cell Int.* **2013**, *13*, No. 89.
(37) Zelikin, A. N.; Quinn, J. F.; Caruso, F. Disulfide cross-linked polymer capsules: En route to biodeconstructible systems. *Biomacromolecules* **2006**, *7*, 27−30.
(38) Zelikin, A. N.; Li, Q.; Caruso, F. Disulfide-stabilized poly(methacrylic acid) capsules: Formation, cross-linking, and degradation behavior. *Chem. Mater.* **2008**, *20*, 2655−2661.
(39) Kempe, K.; Ng, S. L.; Gunawan, S. T.; Noi, K. F.; Caruso, F. Intracellularly Degradable Hydrogen-Bonded Polymer Capsules. *Adv. Funct. Mater.* **2014**, *24*, 6187−6194.
(40) Kempe, K.; Noi, K. F.; Ng, S. L.; Mullner, M.; Caruso, F. Multilayered polymer capsules with switchable permeability. *Polymer* **2014**, *55*, 6451−6459.
(41) Best, J. P.; Neubauer, M. P.; Javed, S.; Dam, H. H.; Fery, A.; Caruso, F. Mechanics of pH-Responsive Hydrogel Capsules. *Langmuir* **2013**, *29*, 9814−9823.
(42) Yildirim, A.; Chattaraj, R.; Blum, N. T.; Goldscheitter, G. M.; Goodwin, A. P. Stable Encapsulation of Air in Mesoporous Silica Nanoparticles: Fluorocarbon-Free Nanoscale Ultrasound Contrast Agents. *Adv. Healthcare Mater.* **2016**, *5*, 1290−1298.
(43) Liberman, A.; Martinez, H. P.; Ta, C. N.; Barback, C. V.; Mattrey, R. F.; Kono, Y.; Blair, S. L.; Trogler, W. C.; Kummel, A. C.; Wu, Z. Hollow silica and silica-boron nano/microparticles for contrast-enhanced ultrasound to detect small tumors. *Biomaterials* **2012**, *33*, 5124−5129.
(44) Elsner, N.; Kozlovskaya, V.; Sukhishvili, S. A.; Fery, A. pH-Triggered softening of crosslinked hydrogen-bonded capsules. *Soft Matter* **2006**, *2*, 966−972.
(45) Ophir, J.; Alam, S. K.; Garra, B.; Kallel, F.; Konofagou, E.; Krouskop, T.; Varghese, T. Elastography: ultrasonic estimation and imaging of the elastic properties of tissues. *Proc. Inst. Mech. Eng., Part H* **1999**, *213*, 203−233.
(46) Wang, X.; Yu, X.; Wang, X. S.; Qi, M. Y.; Pan, J.; Wang, Q. G. One-Step Nanosurface Self-Assembly of D-Peptides Renders Bubble-Free Ultrasound Theranostics. *Nano Lett.* **2019**, *19*, 2251−2258.
(47) Croissant, J. G.; Fatieiev, Y.; Almalik, A.; Khashab, N. M. Mesoporous Silica and Organosilica Nanoparticles: Physical Chemistry, Biosafety, Delivery Strategies, and Biomedical Applications. *Adv. Healthcare Mater.* **2018**, *7*, No. 1700831.
(48) Croissant, J. G.; Fatieiev, Y.; Khashab, N. M. Degradability and Clearance of Silicon, Organosilica, Silsesquioxane, Silica Mixed Oxide, and Mesoporous Silica Nanoparticles. *Adv. Mater.* **2017**, *29*, No. 1604634.
(49) Kesarwani, V.; Kelly, H. G.; Shankar, M.; Robinson, K. J.; Kent, S. J.; Traven, A.; Corrie, S. R. Characterization of Key Bio-Nano Interactions between Organosilica Nanoparticles and Candida albicans. *ACS Appl. Mater. Interfaces* **2019**, *11*, 34676−34687.
(50) Alford, R.; Simpson, H. M.; Duberman, J.; Hill, G. C.; Ogawa, M.; Regino, C.; Kobayashi, H.; Choyke, P. L. Toxicity of Organic Fluorophores Used in Molecular Imaging: Literature Review. *Mol. Imaging* **2009**, *8*, No. 00031.
(51) Mahmoud, A. M.; de Jongh, P.; Briere, S.; Chen, M.; Nowell, C. J.; Johnston, A. P. R.; Davis, T. P.; Haddleton, D. M.; Kempe, K. Carboxylated Cy5-Labeled Comb Polymers Passively Diffuse the Cell Membrane and Target Mitochondria. *ACS Appl. Mater. Interfaces* **2019**, *11*, 31302−31310.
(52) Simpson, J. D.; Smith, S. A.; Thurecht, K. J.; Such, G.Engineered Polymeric Materials for Biological Applications: Overcoming Challenges of the Bio-Nano Interface. *Polymers* **2019**, *11* DOI: 10.3390/polym11091441.